Journal of Coordination Chemistry

ISSN: 0095-8972 (Print) 1029-0389 (Online) Journal homepage: http://www.tandfonline.com/loi/gcoo20

Visible light transformation of Rhodamine 6G using tetracarbazole zinc phthalocyanine when embedded in electrospun fibers and in the presence of ZnO and Ag particles

Phindile Khoza & Tebello Nyokong

To cite this article: Phindile Khoza & Tebello Nyokong (2015) Visible light transformation of Rhodamine 6G using tetracarbazole zinc phthalocyanine when embedded in electrospun fibers and in the presence of ZnO and Ag particles, Journal of Coordination Chemistry, 68:7, 1117-1131, DOI: 10.1080/00958972.2015.1013944

To link to this article: http://dx.doi.org/10.1080/00958972.2015.1013944

Accepted author version posted online: 02 Feb 2015.
Published online: 27 Feb 2015.

Journal of Coordination Chemistry, 2015
Vol. 68, No. 7, 1117–1131, http://dx.doi.org/10.1080/00958972.2015.1013944

Visible light transformation of Rhodamine 6G using tetracarbazole zinc phthalocyanine when embedded in electrospun fibers and in the presence of ZnO and Ag particles

PHINDILE KHOZA and TEBELLO NYOKONG*

Department of Chemistry, Rhodes University, Grahamstown, South Africa

(*Received 6 September 2014; accepted 9 January 2015*)

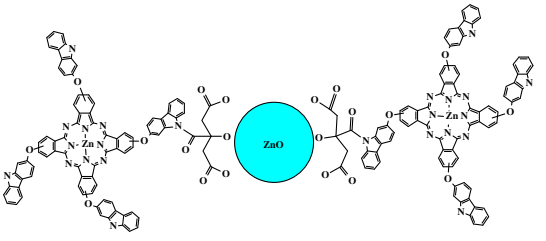

Herein, we report the photocatalytic transformation of Rhodamine 6G (Rh 6G) using tetracarbazole zinc phthalocyanine (TCbZnPc) when alone or when conjugated with ZnO macroparticles (ZnOMPs) and silver nanoparticles (AgNPs), represented as TCbZnPc–ZnOMPs and TCbZnPc–AgNPs, respectively. The photocatalysts were supported onto electrospun polystyrene fibers. The efficiency of TCbZnPc was improved by the presence of both ZnOMPs and AgNPs. HPLC equipped with UV–vis was used to study phototransformation products. The mechanism of transformation was via the N-de-ethylation of Rh 6G.

Keywords: Rhodamine 6G; Photocatalysis; Nanoparticles; Zn-phthalocyanine

1. Introduction

Advanced oxidation process is receiving popularity due to its proficiency in the degradation of recalcitrant dye pollutants in waste water [1–3]. The method is based on the use of reactive oxygen species (ROS) in mineralizing pollutants in water [3, 4]. Photocatalysis is one method for degradation of dye pollutants via ROS generation. The efficiency of the method is mainly dependent on the type of photocatalyst employed [5–7].

*Corresponding author. Email: t.nyokong@ru.ac.za

There have been reports on the use of phthalocyanines (Pcs) as photocatalysts for the phototransformation of organic dyes [8–12]. Photocatalytic applications of Pcs arise from their ability to produce ROS upon irradiation with the appropriate wavelength of light [10, 13, 14]. On the other hand, nanoparticles such as ZnO and TiO_2 are important photocatalysts [15–18]. The mechanism of phototransformation of pollutants by these nanoparticles is reported in the literature [19–21]. However, the downside of using TiO_2 or ZnO as photocatalysts is that they absorb in the UV region of the spectrum. The UV radiation reaching the earth is only 4–6% of the solar irradiation, while 45% constitutes visible light [22], hence the use of visible light in this work and Pcs as photocatalysts since they absorb in the visible region. Even though ZnO is a known photocatalyst, its activity is limited to the UV region and has no activity in the visible region. ZnO (as ZnO macroparticles, ZnOMPs) is used in this work to enhance photocatalytic activity of Pcs in the visible region in the same way as silver nanoparticles (AgNPs) enhance activity due to the heavy atom effect. The heavy atoms (i.e. Ag in AgNPs or Zn in ZnOMPs) encourage the spin–forbidden transition from the singlet to the triplet excited state. The increase in the population of the triplet state as a result of the presence of a high molecular weight element is known as the heavy atom effect; the process occurs as a consequence of spin–orbit coupling [23]. The heavy atom effect increases the triplet quantum yield, which subsequently increases the production of singlet oxygen.

In this work, we employ 2,(3)-tetra(carbazol-2-yloxy)phthalocyaninato zinc(II) (TCbZnPc), figure 1(a), as a photocatalyst for the transformation of Rhodamine 6G (Rh 6G), a model organic dye. A carbazole substituent was chosen since it enhances singlet oxygen production of ZnPc [24]. The use of Pcs containing non–transition metals such as Zn, and excitation in the visible region are expected to result in efficient excitation of the Pc to the triplet state followed by generation of large amounts of ROS.

The effect of ZnO microparticles (ZnOMPs) and Ag nanoparticles (AgNPs) on the efficiency of the phototransformation process is examined. The sizes of the ZnOMPs are in the micrometer range, hence termed microparticles. TCbZnPc and its conjugates with ZnOMPs (TCbZnPc–ZnOMPs), as well as their incorporation into electrospun fibers have been

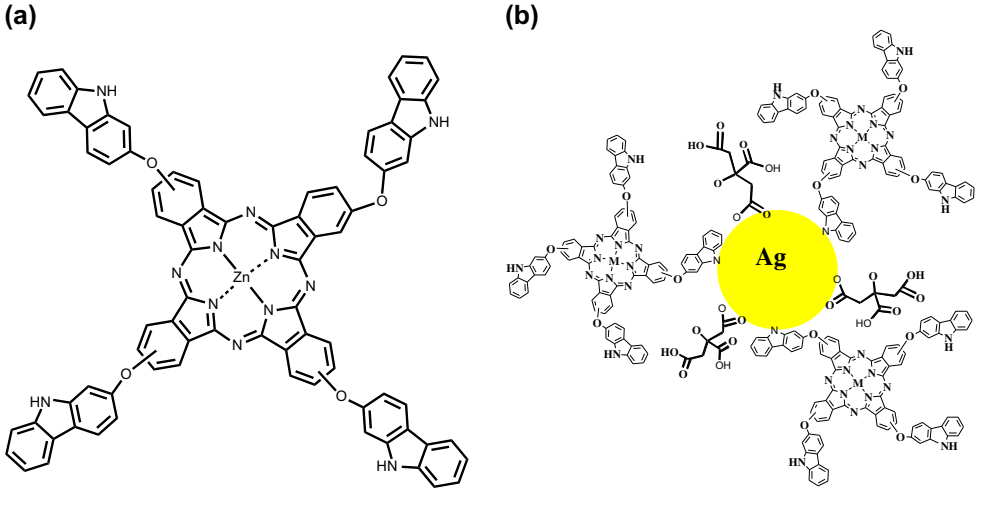

Figure 1. (a) Molecular structure of tetracarbazole derivatized ZnPc (TCbZnPc) used as a photocatalyst upon conjugation and electrospinning into fibers. (b) The illustration of the conjugation of TCbZnPc to AgNPs.

reported [24]. We now report on the use of the TCbZnPc–ZnOMP-modified fibers for the photocatalytic transformation of Rh 6G. We compare the effect of ZnOMPs with that of AgNPs on the photocatalytic activity of the carbazole-derivatized phthalocyanine. AgNPs have been found to improve the photophysicochemical behavior of Pcs [25, 26]. The prepared photocatalysts are immobilized on electrospun fibers for ease of recovery and recyclability.

2. Experimental

2.1. *Materials*

Rh 6G, polystyrene (PS, Mw = 192,000 g M^{-1}), anthracene-9,10–bis-methylmalonate (ADMA) and pH 9.2 buffer tablets were obtained from Sigma Aldrich. Dimethylsulfoxide (DMSO), dimethylformamide (DMF) and tetrahydrofuran (THF) were from SAARCHEM. Acetonitrile was from B & M Scientific. The synthesis of ZnOMPs was reported [24]. The synthesis of 2,(3)-tetra(carbazol-2-yloxy)phthalocyaninatozinc(II), its conjugation with ZnOMPs, and incorporation into electrospun nanofibers were reported recently [24]. AgNPs were also synthesized as reported [27].

2.2. *Equipment*

Ground-state absorption spectra were recorded on a Shimadzu UV-2550 spectrophotometer. Transmission electron microscope (TEM) images were obtained using a Carl Zeiss Libra transmission electron microscope at 100-kV accelerating voltage. Scanning electron microscope (SEM) images were obtained using a JOEL JSM 840 scanning electron microscope.

Photocatalysis (or singlet oxygen quantum yield) experiments were conducted in aqueous media using a General Electric Quartz line lamp (300 W). A 600-nm glass cut-off filter (Schott) and a water filter were used to filter off ultraviolet and infrared radiations, respectively. An interference filter (Intor, 670 nm with a band width of 40 nm) was additionally placed in the light path before the sample. Light intensities were measured with a POWER MAX 5100 (Molectron detector incorporated) power meter and were found to be 9.53×10^{18} photons s^{-1} cm^{-2}. Rh 6G transformation products were profiled on high-performance liquid chromatography (HPLC), by comparison with the retention time of Rh 6G at $t = 0$ s. An Agilent HPLC 1200 series (Agilent Technologies Inc., Germany), equipped with a quaternary pump (G1311A), an auto-sampler (G1329A), a diode array detector (DAD SL G1315C) and a degasser unit (G1322A) was employed. An Eclipse XBD-C18 (i.e. 4.6 mm × 150 mm; 5 μm) column was used for separation of intermediates. The eluting solvent used was 60% water and 40% acetonitrile and the flow rate was kept at 1 mL min^{-1} for 10 min. The flow rate used was 0.8 mL min^{-1} and the injection volume was 25 μl. Absorption spectra were measured at 520 nm by an Agilent DAD UV–vis detector.

2.3. *Photocatalytic reaction*

The modified fiber (10 mg) was suspended in aqueous solution (pH 2 and 9.2) containing Rh 6G. The irradiation experiments were carried out using the photolysis set-up described above. The transformation of Rh 6G was monitored by observing the absorption band of Rh 6G after each photolysis cycle of 10 min, using a Shimadzu UV-2550 spectrophotometer.

2.4. *Synthesis of TCbZnPc–AgNP conjugate*

AgNPs (5 mg) and TCbZnPc (2 mg) were dissolved in 3 mL of DMF, and stirred at room temperature for 96 h. The conjugate was purified by passing through a biobeads column with DMF as an eluent.

2.5. *Preparation of electrospun fibers*

Electrospun nanofibers were prepared as follows: A mixture containing 2.5 g of PS, 3 mg of sample (TCbZnPc–AgNPs or TCbZnPc), and 10 mL DMF/THF(4 : 1) was stirred for 24 h to produce a homogeneous solution. The solution was then placed in a syringe fitted with a capillary needle. A potential difference of 20 kV was applied between the anode and cathode. The distance between the cathode (static fiber collection point) and anode (tip of capillary needle) was 15 cm. The pump rate was maintained at 0.05 mL h^{-1}. The modified fibers are represented as TCbZnPc/PS, TCbZnPc–AgNPs/PS, and TCbZnPc–ZnOMPs/PS. ZnOMPs and AgNPs were also electrospun into PS without TCbZnPc as control and are represented as ZnOMPs/PS and AgNPs/PS, respectively.

2.6. *Determination of singlet oxygen quantum yields*

Singlet oxygen quantum yield studies have been reported for TCbZnPc–ZnOMPs/PS and TCbZnPc/PS [24]. A chemical method was used to determine singlet oxygen quantum yield for TCbZnPc–AgNPs/PS. The studies were carried out in an aqueous solution, using ADMA (concentration = 3.33×10^{-5} M) as a chemical quencher for singlet oxygen. The decrease in the absorption of ADMA at 380 nm was monitored. The modified fiber (20 mg) was suspended in a solution containing ADMA, and irradiated using the photolysis set-up described above. The singlet oxygen quantum yields were calculated using equation (1) as described [8]:

$$\frac{1}{\phi_{\mathrm{ADMA}}} = \frac{1}{\phi_{\Delta}} + \frac{1}{\phi_{\Delta}} \frac{k_{\mathrm{d}}}{k_{\mathrm{a}}} \frac{1}{[\mathrm{ADMA}]} \tag{1}$$

where k_{d} is the decay constant of singlet oxygen, k_{a} is the rate constant of the reaction of ADMA with O_2 ($^1\Delta_g$), and ϕ_{ADMA} is the quantum yield for transformation of ADMA. The intercept obtained from the plot of $1/\phi_{\mathrm{ADMA}}$ *versus* 1/[ADMA] gives the ϕ_{Δ} values. The derivation of this equation uses the absorbance of the metallophthalocyanines (MPcs) on the fiber. The light intensity measured refers to the light reaching the spectrophotometer cell; it is expected that some of the light may be scattered; hence, the ϕ_{Δ} values of the MPcs in the fibers are estimates. We have previously proved the light scattering effects of PS fibers using UV–vis spectra of Pcs, where an increase in the absorption, due to the fiber, was observed from 600 nm [8].

3. Results and discussion

3.1. *Characterization of AgNPs and TCbZnPc–AgNPs in solution and in electrospun fibers*

Silver is well known for its high affinity for S and N [28, 29]. The possible interaction between the MPcs and AgNPs may be via the secondary amine of the carbazole, which is achieved by ligand exchange, where some of the citrate capping is replaced by the Pc,

figure 1(b). It is possible for more than one Pc to be coordinated with one AgNP. But the reverse, where more than one AgNP coordinates with a Pc, is unlikely due to size consideration. It is also possible for Pcs to coordinate with each AgNP using more than one of the peripheral substituents, depending on orientation. Thus, figure 1(b) is a hypothetical representation of the conjugate showing some leftover citrate capping on the AgNP and some Pcs conjugated with the AgNP.

3.1.1. TEM and SEM images. The TEM images, of the conjugates, and the corresponding particle size distribution are depicted in figure 2. The TCbZnPc–ZnOMPs were obtained as microflakes as reported before [24] with diameters ranging from 3 to 19 μm [figure 2(a)]. The diameter of the TCbZnPc–AgNPs varied from 5 to 88 nm, figure 2(b). The SEM images of the functionalized electrospun PS fibers are shown in figure 3. The fibers obtained were cylindrical and un-branched with relatively smooth surfaces. The diameter of the fibers ranged from 1 to 8 μm, with no significant increase in the fiber diameter upon functionalization with Pc or its conjugate with AgNPs.

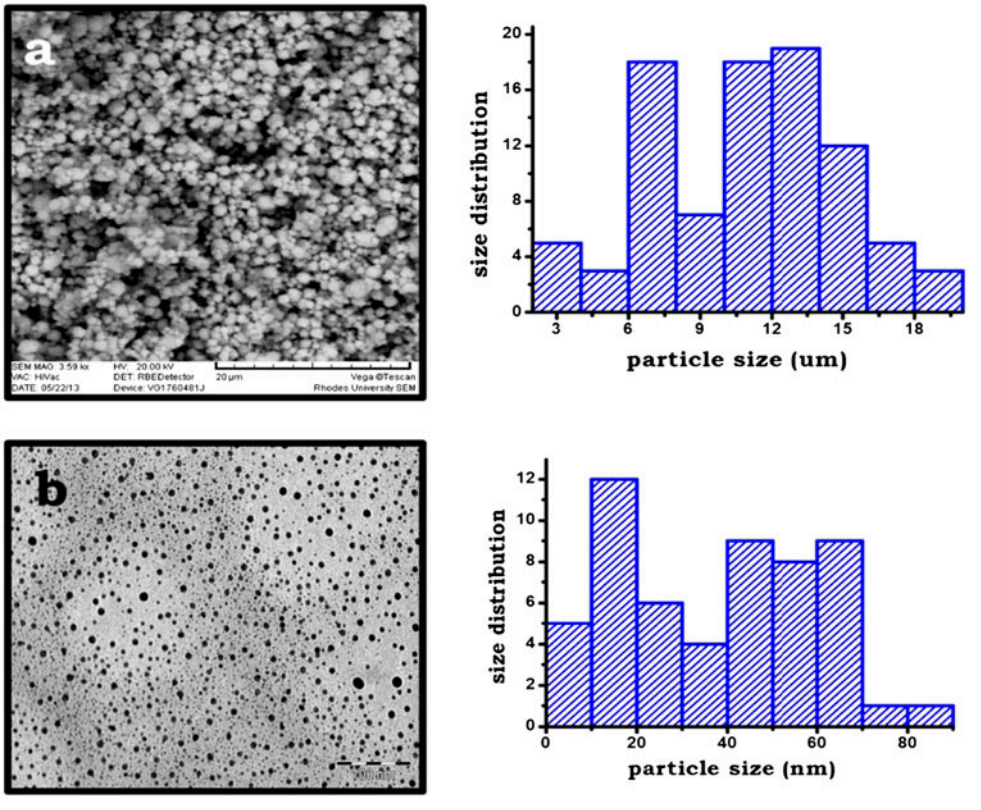

Figure 2. TEM images, with the corresponding particles size distribution, of TCbZnPc-ZnOMPs (a) and TCbZnPc-AgNPs (b).

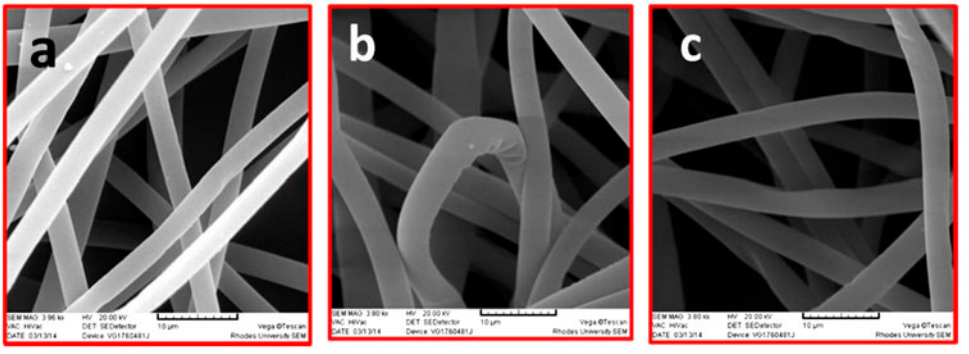

Figure 3. SEM images of the electrospun PS alone (a), TCbZnPc (b), TCbZnPc-AgNPs (c).

3.1.2. UV–vis spectra. Figure 4 shows the UV–vis of AgNPs, TCbZnPc alone and when conjugated with AgNPs. An intense, and sharp surface plasmonic resonance (SPR), typical of AgNPs appeared at ~430 nm. In the presence of the Pc, there was clear red shift and broadening of the SPR band, attributed to aggregation of AgNPs upon conjugation. Aggregation results in red shifting of the SPR band [30]. There is no significant shift in the Q-band of the TCbZnPc in the presence of AgNPs, only broadening below 600 nm due to the SPR band of the AgNPs.

3.1.3. Singlet oxygen quantum yields. The singlet oxygen quantum yields of the functionalized fiber were determined by the absolute method with ADMA as the singlet oxygen quencher. Figure 5 shows the transformation profile of ADMA using TCbZnPc/PS. The figure shows a decrease in the ADMA absorption as it reacts with singlet oxygen generated by the TCbZnPc. Equation (1) was employed to determine singlet oxygen quantum yields from figure 5. As expected, the singlet oxygen quantum yields were higher on conjugating AgNPs, table 1. Singlet oxygen quantum yield values were determined to be 0.25 [24], 0.28 and 0.20 [24] for TCbZnPc/PS, TCbZnPc–AgNPs/PS and TCbZnPc–ZnOMPs/PS, respectively, table 1.

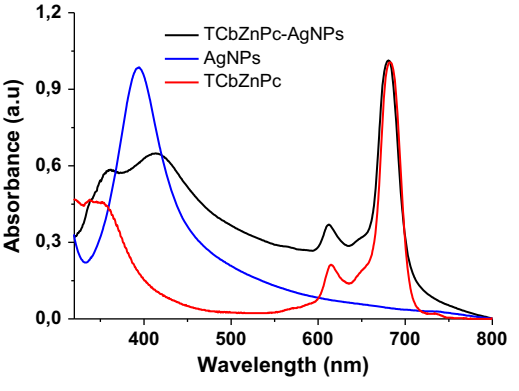

Figure 4. UV–vis spectra of AgNPs, TCbZnPc, TCbZnPc-AgNPs in DMSO as a solvent.

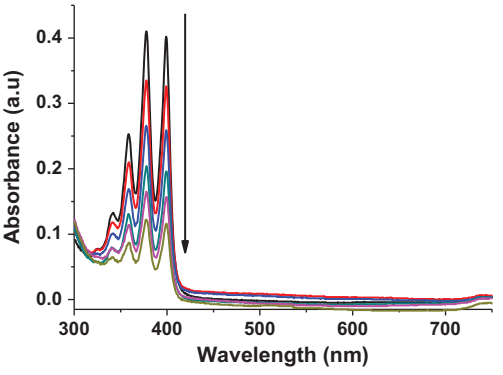

Figure 5. Transformation profile of ADMA (3.33×10^{-5} M) using TCbZnPc-AgNPs/PS in water.

3.2. *Phototransformation of Rh 6G*

3.2.1. Spectroscopic studies. To assess the efficiency of the prepared photocatalysts, the phototransformation of Rh 6G was used as a test model. Figure 6 shows the spectral changes of Rh 6G upon illumination in the presence of TCbZnPc/PS, under pH 9.2 conditions. Similar spectral changes were observed for TCbZnPc–ZnOMPs/PS or TCbZnPc–AgNPs/PS. As can be seen in figure 6, the maximum absorption at 525 nm gradually decreased with time. There was no significant decrease in the Rh 6G peak on photolysis in the absence of TCbZnPc–ZnOMPs/PS, TCbZnPc–AgNPs/PS or TCbZnPc/PS. There was, however, a noticeable blue shifting of the Rh 6G peak with time (figure 6). According to Chen *et al.,* this blue shift in absorption spectra is related to the N-de-ethylation of Rhodamine B [31], with the magnitude of the shift dependent on the photocatalyst employed. Scheme 1(b) shows the N-de-ethylation of Rh 6G, following generation of singlet oxygen by TCbZnPc in scheme 1(a).

Experiments using ZnOMPs/PS or AgNPs/PS were also performed, but there were negligible changes on the Rh 6G peak on excitation with visible light since ZnOMPs absorb strongly in the UV region. Irradiation in this study was done only in the visible region, so photocatalytic behavior is not expected of ZnOMPs. It is proposed that the role of the AgNPs and ZnOMPs is to increase the production of ROS, hence increase the phototransformation rate of Rh 6G. For TCbZnPc–AgNPs/PS, an increase in the singlet oxygen quantum yield is observed in table 1 compared with TCbZnPc/PS alone. For TCbZnPc–ZnOMPs/PS, there is a decrease in singlet oxygen quantum yield compared with TCbZnPc; however, other ROS are generated as shown in scheme 2. Photolysis with the electrospun polystyrene (without TCbZnPc–ZnOMPs, TCbZnPc–AgNPs, or TCbZnPc as photocatalysts) using visible light had no effect on Rh 6G transformation. The results indicate that the transformation of Rh 6G is largely initiated by the ROS produced upon exciting the phthalocyanine.

3.2.2. Kinetics. Effluent from the textile industry is discharged to the environment at different pHs. Thus, the efficiency of a photocatalyst needs to be examined under different pH conditions. In our study, two different pHs, acidic (pH 2) and basic (pH 9.2), were used to determine the photocatalytic activity of the TCbZnPc/PS TCbZnPc–AgNPs/PS and TCbZnPc–ZnOMPs/PS fibers. The plots of Rh 6G concentration *versus* time are shown in

Table 1. Kinetic data of transformation of Rh 6G using the unmodified and hybrid photocatalyst. Excitation wavelength = 670 nm.

	ϕ_Δ	pH 2			pH 9.2		
		k_{obs} (min^{-1})	Initial-rate × 10^{-8} (M L^{-1} min^{-1})	Half-life (min)	k_{obs} (min^{-1})	Initial-rate × 10^{-8} (mol L^{-1} min^{-1})	Half-life (min)
TCbZnPc/Ps	0.25[a]	0.0105	5.71	66.0	0.0131	7.07	52.9
TCbZnPc-ZnOMPs/Ps	0.20[a]	0.00467	2.51	148	0.0153	8.25	45.3
TCbZnPc-AgNPs/Ps	0.28	0.0189	10.18	36.6	0.0312	16.8	22.2

[a]Values from Ref. [24].

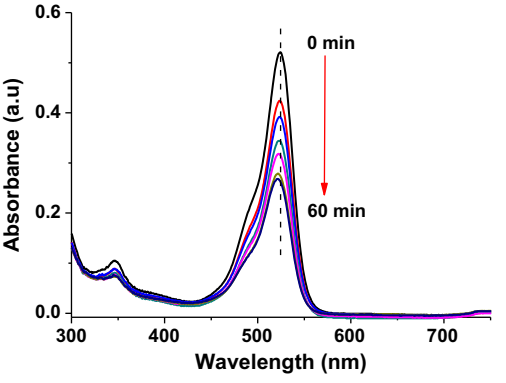

Figure 6. Spectral changes observed during the phototransformation of Rh 6G, with TCbZnPc/PS as a catalyst under pH 2 conditions. Time interval = 10 min.

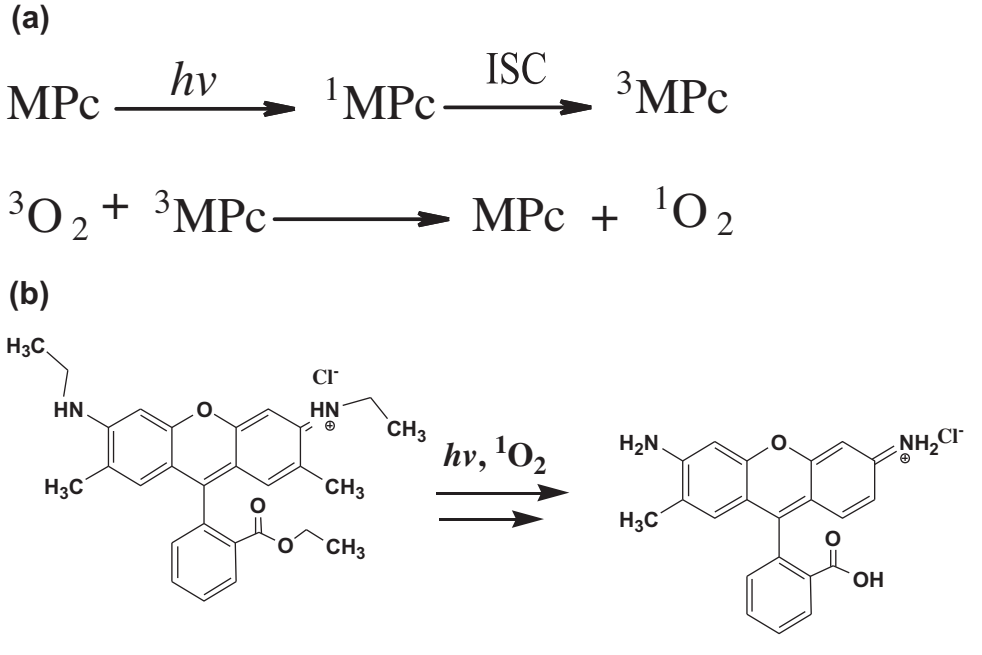

Scheme 1. (a) Generation of singlet oxygen by TCbZnPc photocatalyst and (b) de-ethylation of Rh 6G.

figure 7, and the kinetic data obtained from these plots are presented in table 1. The linearity of the plots obtained, from the ln (C_0/C_t) *versus* time, indicates that the reactions follow pseudo-first-order kinetics. The rate (k_{obs}) of transformation of TCbZnPc–AgNPs/PS was larger than that of TCbZnPc/PS under both pH 2 and 9.2 conditions, when the concentration was 5.36 μM, table 1.

When the pH was 9.2, the presence of both particles (AgNPs or ZnOMPs) greatly enhanced the photocatalytic activity of TCbZnPc/PS, attributed to increased hydroxyl radicals under this pH [32]. While k_{obs} remained higher for TCbZnPc–AgNPs/PS

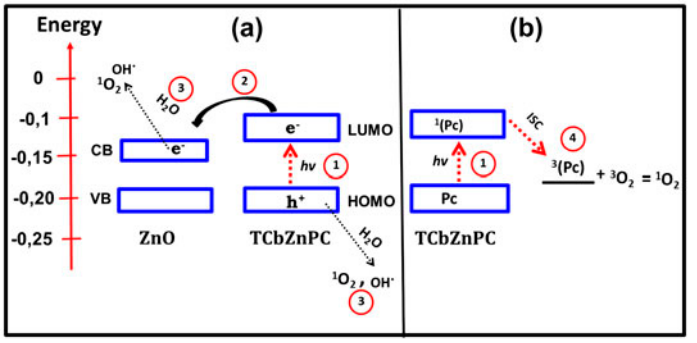

Scheme 2. Formation of ROS by photosensitization of ZnO upon exciting the Pc with the UV light. VB = valence band, CB = conduction band, HOMO = highest occupied molecular orbital, LUMO = lowest occupied molecular orbital.

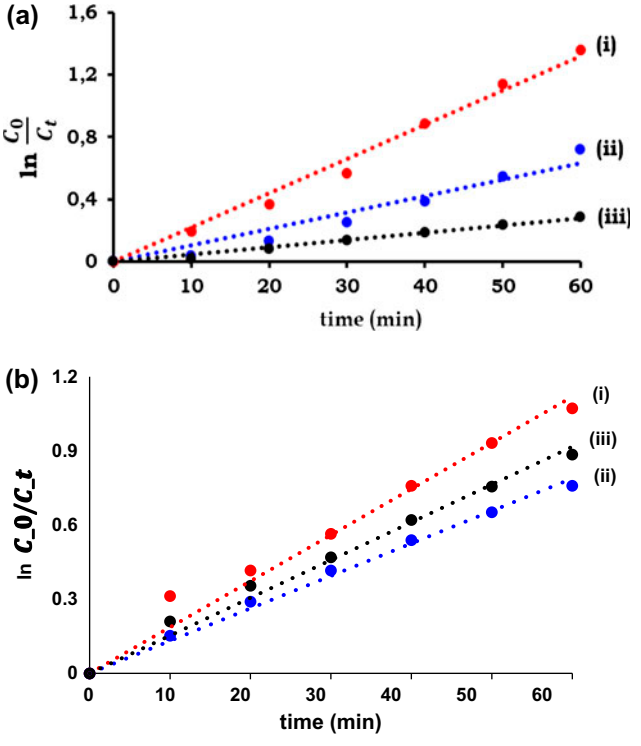

Figure 7. First order kinetic plots for the phototransformation of Rh 6G under pH 9.2 (a) and pH 2 conditions (b), with TCbZnPc-AgNPs (i), TCbZnPc-ZnOMPs (ii), TCbZnPc (iii) as photocatalysts.

(compared with TCbZnPc/PS) under acidic conditions, there was a reduction in the transformation rate of Rh 6G with TCbZnPc–ZnOMPs/PS as a photocatalyst. The low transformation efficiency at low pHs is attributed to dissolution and photodissolution of ZnO under acidic conditions [33].

Studying the dependence of transformation efficiency on the initial dye concentration is important from an application point of view [34]. Table 2 shows the effect of the initial Rh 6G concentration on its photocatalytic transformation at pH 9.2.

In the presence of all prepared photocatalysts, the reaction rates (k_{obs}) decreased with an increase in the concentration of Rh 6G. As the concentration of Rh 6G increases, the path length of the photons entering the solution decreases, reducing the rates of Rh 6G photo-transformation at higher concentrations. The reverse is true at lower concentrations where there is an increase in the number of photons absorbed by the catalyst, resulting in increased rates [35]. The same effect was observed by Wang *et al.* [35] during photocatalytic decolorization of commercial dyes using zinc oxide powder as photocatalyst.

The influence of initial dye concentration on photocatalytic transformation with a heterogeneous system is described by the Langmuir–Hinshelwood kinetic model [36], equation (2):

$$\frac{1}{r^0} = \frac{1}{kK_A}\frac{1}{C_0} + \frac{1}{k} \tag{2}$$

where k is the apparent reaction rate constant, K_A is the adsorption coefficient, and C_0 corresponds to the initial concentration of Rh 6G. Plots of the inverse of initial reaction rate *versus* the reciprocal of the initial concentration of Rh 6G were linear with non-zero intercepts, figure 8 (using TCbZnPc–AgNPs/PS and TCbZnPc/PS as examples, a similar plot was obtained for TCbZnPc–ZnOMPs/PS with data shown in table 3). The results presented in figure 8 give an indication that the Langmuir–Hinshelwood kinetic model is the appropriate model for describing the phototransformation of Rh 6G in the presence of functionalized fibers. Therefore, it can be deduced that catalysis occurs at the surface of the supported photocatalyst.

The adsorption coefficient (K_A) for all the functionalized fibers was determined from the slope in figure 8, and was found to be, 49.87, 24.15, and 31.76 $(M\ L^{-1})^{-1}$ for TCbZnPc/PS, TCbZnPc–AgNPs/PS, and TCbZnPc–ZnOMPs/PS, respectively, table 3. A high adsorption coefficient indicates the tendency of the material to be adsorbed rather than remaining in

Table 2. Kinetic data of transformation of Rh 6G using the unmodified and hybrid photocatalyst at pH 9.2.

Complex[a]	Concentration (μM)	$k_{obs} \times 10^{-2}$ (min^{-1})	Initial rate $\times 10^{-8}$ ($M^{-1}\ min^{-1}$)	Half life (min)
TCbZnPc/Ps (0.25)	2.15	2.11	4.56	32.7
	3.44	1.68	5.78	41.3
	5.39	1.31	7.07	52.9
	8.70	0.934	8.13	74.2
	13.1	0.902	11.8	76.8
TCbZnPc-AgNPs/Ps (0.28)	2.15	3.57	7.70	19.4
	3.44	3.55	12.2	19.5
	5.39	3.12	16.8	22.2
	8.70	2.58	22.4	26.9
	13.1	2.15	28.2	32.1
TCbZnPc-ZnOMPs/Ps (0.20)	2.15	2.61	3.63	41.1
	3.44	2.34	5.08	46.9
	5.39	1.53	8.25	45.3
	8.70	1.15	9.99	60.3
	13.1	0.957	12.5	72.4

[a]Singlet oxygen quantum yields in water in brackets.

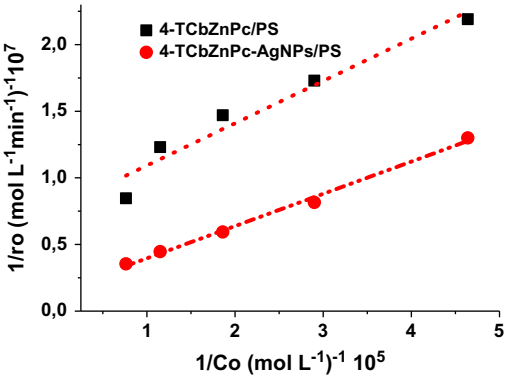

Figure 8. Plots of the reciprocal of the initial reaction rate *vs.* the reciprocal of the initial concentration for transformation of Rhodamine 6G at pH 9.2.

Table 3. Kinetic data of transformation of Rh 6G using the unmodified and hybrid photocatalyst at pH 9.2.

Catalyst	k (M L^{-1} min^{-1}) × 10^{-7}	K_A (M L^{-1})$^{-1}$
TCbZnPc/PS	1.29	49.87
TCbZnPc-AgNPs/PS	6.45	24.15
TCbZnPc-ZnOMPs/PS	2.02	31.73

solution. The adsorption coefficient of TCbZnPc–AgNPs/PS was lower compared with the other functionalized fibers, suggesting that desorption is much more favored in this system.

From the intercept in figure 8, the apparent rate constants k were determined to be 1.29×10^{-7}, 6.45×10^{-7}, and 2.02×10^{-7} M L^{-1} min^{-1} for TCbZnPc/PS, TCbZnPc–AgNPs/PS, and TCbZnPc–ZnOMPs/PS, respectively, table 3. The reaction rate was enhanced by the presence of AgNPs over ZnOMPs.

3.2.3. Mechanisms. Two possible processes may be occurring during the excitation of the phthalocyanine in the presence of ZnO [scheme 2(a) and (b)]: upon excitation with visible light (1), the electron–hole pair is formed in the highest occupied molecular orbital (HOMO) and lowest unoccupied molecular orbital (LUMO) of the phthalocyanine. The electron in the LUMO is then injected into the conduction band of ZnO (2). In the presence of water, the charged species undergo several reactions forming ROS (3). A second possible mechanism involves the intersystem crossing of the excited dye to the forbidden triplet state, with subsequent reactions resulting in the formation of ROS (4), see also scheme 1(A). The heavy atom effect of silver or ZnO enhances the population of the triplet state (4), as explained in the introduction. Thus, Pcs act as co-catalyst (with ZnO), by forming ROS such as singlet oxygen (scheme 2, steps 3 and 4) and others. Therefore, in this work, we combined phthalocyanine with ZnO and Ag for improved photocatalytic behavior, as a result of an increase in ROS formation and the heavy atom effect induced by the presence of Zn and Ag.

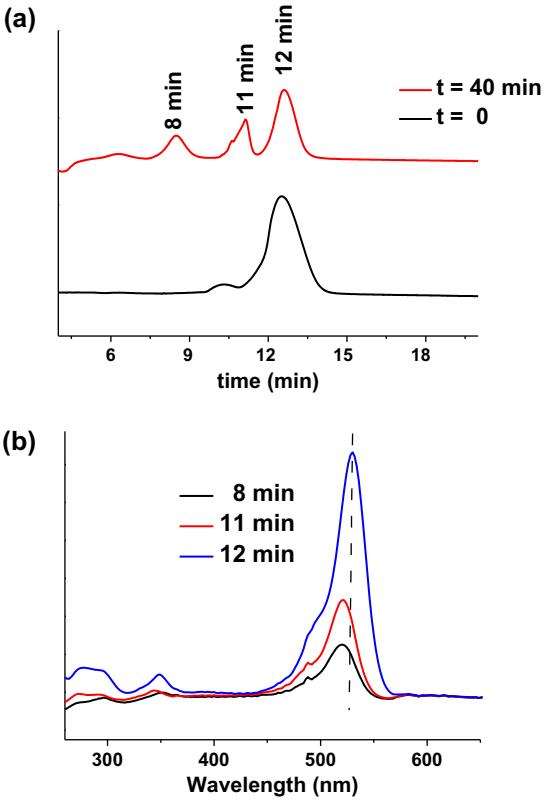

Figure 9. HPLC chromatograms (a) of phototransformation products obtained at $t = 0$ and after 40 min irradiation time, and the UV–vis spectra (b) of the peaks corresponding to 8, 11 and 12 min in the HPLC spectrum obtained at $t = 40$ min. The photocatalyst employed was TCbZnPc at pH 9.2.

3.2.4. Chromatographic analysis. The products of phototransformation were characterized using HPLC, and the chromatograms are shown in figure 9(a). The chromatogram in figure 9(a) shows the appearance of new peaks at 8 and 11 min. The appearance of these new peaks is associated with a decrease in the main Rh 6G peak at 12 min. UV–vis spectra of the phototransformation products at $t = 11$ or 8 min [figure 9(b)] are similar to those of Rh 6G ($t = 12$ min). However, there exist clear hyposochromic shifts of the transformation products from the parent Rh 6G peak. This blue shift has been associated with the N-de-ethylation of Rhodamine [31], scheme 1(b). Rhodamine derivatives are reported to undergo de-ethylation prior to the complete mineralization of the dye [31].

3.2.5. Catalyst stability and recyclability. The stability of the functionalized catalyst (using TCbZnPc/PS) was examined for the phototransformation of Rh 6G during a five-cycle experiment, as shown in figure 10. Prior to each cycle, the catalyst was washed with water and dried at room temperature. Figure 10 shows the percentage phototransformation of Rh 6G using TCbZnPc/PS as an example. The percentage dye phototransformation with time was calculated using equation (3):

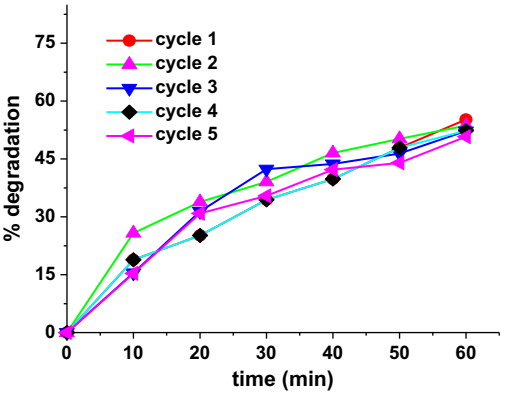

Figure 10. Percentage Rh 6G removal, at pH 2, in the presence of the unmodified photocatalyst (TCbZnPc/PS).

$$\%\,\text{Photodegradation} = \frac{C_0 - C_t}{C_0} \times 100 \tag{3}$$

where C_0 and C_t are Rh 6G concentrations before and at time t after photolysis. Figure 10 shows that photocatalytic activity remained relatively unchanged after each cycle, with no significant changes on the percentage dye transformation. This indicates the stability and efficiency of TCbZnPc/PS for the transformation of Rh 6G under visible light irradiation, and the catalyst could be easily separated for reuse. Similar behavior was observed for the other photocatalysts.

4. Conclusions

Tetracarbazole zinc phthalocyanine (TCbZnPc) is conjugated with macroparticles (ZnOMPs) and AgNPs, represented as TCbZnPc–ZnOMPs and TCbZnPc-ZnOAgNPs and supported onto electrospun polystyrene fibers. The efficiency of TCbZnPc was improved by the presence of both ZnOMPs and AgNPs under basic conditions, while the efficiency of the hybrid catalysts (TCbZnPc–ZnOMPs) was greatly reduced under acidic conditions. HPLC equipped with UV–vis was used to study the phototransformation products. The mechanism of transformation was via the N-de-ethylation of Rh 6G, proven by the blue shift of the Rh 6G peak with an increase in irradiation time. The catalysts showed excellent reusability.

Funding

This work was supported by the Department of Science and Technology (DST) Innovation and National Research Foundation (NRF), South Africa through DST/NRF South African Research Chairs Initiative for Professor of Medicinal Chemistry and Nanotechnology (UID 62620) as well as Rhodes University and DST/Mintek Nanotechnology Innovation Centre (NIC) – Sensors, South Africa.

References

[1] R. Andreozzi, V. Caprio, A. Insola, R. Marotta. *Catal. Today*, **53**, 51 (1999).
[2] M. Pera-Titus, V. García-Molina, M.A. Baños, J. Giménez, S. Esplugas, *Appl. Catal., B*, **47**, 219 (2004).
[3] P.Y. Chan, M. Gamal El-Din, J.R. Bolton. *Water Res.*, **46**, 5672 (2012).
[4] R. Munter. *Proc. Est. Acad. Sci. Chem.*, **50**, 59 (2001).
[5] T. Robinson, G. McMullan, R. Marchant, P. Nigam. *Bioresour. Technol.*, **77**, 247 (2001).
[6] E. Neyens, J. Baeyens. *J. Hazard. Mater.*, **98**, 33 (2003).
[7] E. Forgacs, T. Cserháti, G. Oros. *Environ. Int.*, **30**, 953 (2004).
[8] R. Zugle, E. Antunes, S. Khene, T. Nyokong. *Polyhedron*, **33**, 74 (2012).
[9] S. Tombe, E. Antunes, T. Nyokong. *J. Mol. Catal. A Chem.*, **371**, 125 (2013).
[10] R. Zugle, T. Nyokong. *J. Appl. Polym. Sci.*, **128**, 1131 (2013).
[11] S. Wang, Y. Fang, Y. Yang, J. Liu, A. Deng, X. Zhao, Y. Huang. *Chinese Sci. Bull.*, **56**, 969, (2011).
[12] H. Golmojdeh, M.A. Zanjanchi, M. Arvand. *Photochem. Photobiol.*, **89**, 1029 (2013).
[13] C.M. Whitacre, D.K. Feyes, T. Satoh, J. Grossmann, J.W. Mulvihill, H. Mukhtar, N.L. Oleinick. *Clin. Cancer Res.*, **6**, 2021 (2000).
[14] D. Jančula, L. Bláhová, M. Karásková, B. Maršálek. *Water Sci. Technol.*, **62**, 273 (2010).
[15] R.T. Tayade, P.K. Surolia, R.G. Kulkarni, R.V. Jasra. *Sci. Technol. Adv. Mater.*, **8**, 455 (2007).
[16] Q.I. Rahman, M. Ahmad, S.K. Misra, M. Lohani. *Mater. Lett.*, **91**, 170 (2013).
[17] C. Yu, K. Yang, Y. Xie, Q. Fan, J.C. Yu, Q. Shu, C. Wang. *Nanoscale*, **5**, 2142 (2013).
[18] U.I. Gaya, A.H. Abdullah. *J. Photochem. Photobiol. C*, **9**, 1 (2008).
[19] D.S. Bhatkhande, V.G. Pangarkar, A.A.C.M. Beenakers. *J. Chem. Technol. Biotechnol.*, **77**, 102 (2001).
[20] U.G. Akpan, B.H. Hameed. *J. Hazard. Mater.*, **170**, 520 (2009).
[21] I.K. Konstantinou, T.A. Albanis. *Appl. Catal. B*, **49**, 1 (2004).
[22] C. Wang, J. Li, G. Mele, G.-M. Yang, F.-X. Zhang, L. Palmisano, G. Vasapollo. *Appl. Catal. B*, **76**, 218 (2007).
[23] J. Koziar, D. Cowan. *Acc. Chem. Res.*, **11**, 334 (1978).
[24] P. Khoza, E. Antunes, T. Nyokong. *Dyes Pigm.*, **104**, 57 (2014).
[25] N. Rapulenyane, E. Antunes, T. Nyokong. *New J. Chem.*, **37**, 1216 (2013).
[26] N. Masilela, E. Antunes, T. Nyokong. *J. Porphyrins Phthalocyanines*, **17**, 417 (2013).
[27] A. Henglein, M. Giersig. *J. Phys. Chem. B*, **103**, 9533 (1999).
[28] J.D. Lamb, A.Y. Nazarenko, J. Uenishi, H. Tsukube. *Anal. Chim. Acta*, **373**, 167 (1998).
[29] A.F. Danil de Namor, O.E. Piro, L.E. Pulcha Salazar, A.F. Aguilar-Cornejo, N. Al-Rawi, E.E. Castellano, F.J. Sueros Velardea. *J. Chem. Soc. Faraday Trans.*, **94**, 3097 (1998).
[30] S. He, J. Yao, P. Jiang, D. Shi, H. Zhang, S. Xie, S. Pang, H. Gao. *Langmuir*, **17**, 1571 (2001).
[31] F. Chen, J. Zhao, H. Hidaka. *Int. J. Photoenergy*, **5**, 209 (2003).
[32] S.-M. Lam, J.-C. Sin, A.Z. Abdullah, A.R. Mohamed. *Desalin. Water Treat.*, **41**, 131 (2012).
[33] J.Z. Kong, A.D. Li, X.Y. Li, H.F. Zhai, W.Q. Zhang, Y.P. Gong, H. Li, D. Wu. *J. Solid State Chem.*, **183**, 1359 (2010).
[34] N. Sobana, M. Swaminathan. *Sol. Energy Mater. Sol. Cells*, **91**, 727 (2007).
[35] H. Wang, C. Xie, W. Zhang, S. Cai, Z. Yang, Y. Gui. *J. Hazard. Mater.*, **141**, 645 (2007).
[36] M.A. Fox, M.T. Dulay. *Chem. Rev.*, **93**, 341 (1993).